Research article

Prognostic role of *MUCIN* family and its relationship with immune characteristics and tumor biology in diffuse-type gastric cancer

Xiao-Xiao Luo [a,**,1], Shi-Zhen Li [b,1], Lu Wang [a], Ai-Lin Luo [c], Hong Qiu [a], Xiang-Lin Yuan [a,*]

[a] Department of Oncology, Tongji Hospital, Tongji Medical College, Huazhong University of Science and Technology, Wuhan 30030, China
[b] Department of Biliary-Pancreatic Surgery, Tongji Hospital, Tongji Medical College, Huazhong University of Science and Technology, Wuhan 30030, China
[c] Department of Anesthesiology, Tongji Hospital, Tongji Medical College, Huazhong University of Science and Technology, Wuhan 430030, Hubei Province, China

ARTICLE INFO

ABSTRACT

The main component of O-glycoproteins, mucin, is known to play important roles in physiological conditions and oncogenic processes, particularly correlated with poor prognosis in different carcinomas. Diffuse-type gastric cancer (DGC) has long been associated with genomic stability and unfavorable clinical outcomes. To investigate further, we obtained clinical information and the RNA-seq data of the TCGA-STAD cohort. Through the use of unsupervised clustering methods and GSEA, we identified two distinct clusters, characterized by higher and lower expression of MUC2 and MUC20, denoted as cluster 1 and cluster 2, respectively. Subsequently, employing CIBERSORT, it was determined that cluster 2 exhibited a higher tumor mutation burden (TMB) and a greater abundance of CD8$^+$ T cells and activated CD4$^+$ memory T cells, in addition to immune checkpoints (ICPs). On the other hand, cluster 1 showed a lower TIDE score estimation, indicating a higher probability of tumor immune escape. Furthermore, overexpression of MUC15 and MUC20 was confirmed through qPCR and Western blotting, and their specific roles in mediating the epithelial-mesenchymal transition (EMT) process of GC cells (SNU484 and Hs746t) were validated via CCK-8 assay and wound healing assay in vitro. These findings highlight the potential prognostic value of MUC20 and offer insights into the prospects of immunotherapy for DGC by targeting MUC20.

1. Introduction

Gastric cancer (GC) has been a major global public health concern due to its high morbidity and mortality rates, accounting for more than half of deaths annually and ranking as the third leading fatal cancer. The prognosis of GC has been found to be correlated with histological characteristics and tumor stage. The World Health Organization (WHO) has classified gastric cancer into diffuse,

intestinal, and mixed types, with the diffuse-type gastric cancer (DGC) consistently associated with the worst outcomes [1,2,3].

Given its genetic and cellular heterogeneity, molecular classifications of GC encompass somatic mutations, gene expressions, clinical features, and outcomes. The Cancer Genome Atlas (TCGA) has distinguished GC into four types—chromosomal instability (CIN), Epstein–Barr virus positive (EBV), microsatellite unstable (MSI), and genome stable (GS). Notably, DGC is predominantly classified as the genome stable (GS) type, indicating genomic stability and a critical need for targeted therapy.[3] The Asian Cancer Research Group (ACRG) has also classified GC into four subtypes associated with distinct clinical prognosis, revealing that DGC is mainly classified as the MSS/EMT subtype, signaling poor clinical outcomes and limited treatment options [4]. The urgent need for effective treatment strategies and personalized medicine for individuals suffering from DGC is evident.

Additionally, mucin, the main component of epithelial cells-expressed O-glycoproteins with diverse biophysiochemical properties, plays a crucial role in both physiological conditions and oncogenic processes [5]. The expression of different mucins has been linked to poor prognosis in various cancers, while the comprehensive evaluation of MUCIN family members in DGC and their role in the immune process remains elusive.

Immunotherapy has revolutionized the paradigm of cancer treatment by aiming to restore immune surveillance and elicit an antitumor response [6,7]. However, responses to immune checkpoint inhibitors (ICIs) and immune cell infiltration (TCIs) in the tumor microenvironment (TME) significantly impact the outcome of immunotherapy [8–10]. Tumors are categorized as 'hot' or 'cold' based on the amount of tumor-infiltrating lymphocytes (TILs), ultimately influencing the effectiveness of immunomodulatory strategies [11–13]. The current clinical guidelines specify programmed death 1 (PD-1) and programmed death ligand 1 (PD-L1) monoclonal antibodies as the ICIs for GC; however, their benefits are limited compared to traditional chemotherapy. One of the key mechanisms underlying immunotherapy resistance is immune evasion, wherein tumor cells evade immune surveillance and elimination in the TME [14–16].

In this context, the study aimed to evaluate the patterns of the MUCIN family in DGC and their relationship with clinical outcomes. The clustering of the MUCIN family members' expression revealed two distinct clusters with differing survival and immunity activation patterns. The analysis of MUCIN expression with immune cell infiltration and the tumor microenvironment aimed to provide insights for the clinical management of DGC and the broader application of immunotherapy.

2. Materials and methods

2.1. Data sources

In this study, clinical information and RNA-seq data of gastric carcinoma were downloaded from the TCGA-STAD cohort (https://portal.gdc.cancer.gov/), with a subset of 375 samples being selected for analysis. Additionally, detailed clinical characteristics and survival information were obtained from the GSE66229 dataset in the gene expression omnibus (GEO) database.

2.2. Data processing and differentially expressed genes selection

First, 63 out of 375 samples were chosen for subsequent analysis as diffuse-type gastric adenocarcinoma. The data of the selected samples on RNA-seq were then CPM transformed using "edgeR" [17]. Following this, the Limma [18] package and Wilcoxon test were employed to identify differentially expressed genes between normal and tumor tissues, with a false discovery rate FC $\geq$ 2 and $p < 0.05$.

2.3. Clustering analysis

The MUC gene family, CLDN gene family, and ZNF gene family were among the regulated genes selected for univariate COX analysis, based on previous reports [19–21]. Following this, the R package "ConsensusClusterPlus" [22] was used to perform consensus clustering of the subtypes within the cohort.

2.4. Survival analysis and construction of nomogram

Using survival packages [23], Kaplan–Meier Plotter (www.kmplot.com) was utilized for overall survival and disease-free survival, with P value 0.05. Univariate logistic regression and multivariable logistic regression was performed. Regression equations were calculated, and nomograms were plotted. Moreover, receiver operating characteristic (ROC) curve was also employed for model evaluation. Finally, decision curves were plotted by calculating the net benefits corresponding to different threshold probabilities.

2.5. Gene set enrichment analysis (GSEA)

Accounting for Gene Ontology (GO) and Kyoto Encyclopedia of Genes and Genomes (KEGG) analyses database [24], we adopted GSEA application (https://www. broadlnstitute. org/gsea/) for detection of changes in expression of genes. Containing valuable information about biological characteristics [25], gene regulatory networks and enriched signaling pathways between clusters were carefully analyzed, with P-value<0.05 and FDR<0.05 defined significant.

2.6. Infiltration level of TIICs

The CIBERSORT deconvolution algorithm (https://cibersort.stanford.edu/) method is adopted to evaluate the proportion of 20 immune cells based on transcriptional data [26]. Wilcox. test was used to for differential estimation on immune infiltration. The *P* value cutoff was 0.05. The ESTIMATE algorithm was applied to calculate immune scores (https://bioinformatics. mdanderson. org/estimate/).

2.7. T cell-inflamed score

T cell-inflamed score defines preexisting cancer immunity and predicts the clinical response of ICB. Eighteen genes and several algorithms are involved in T cell-inflamed score according to gene expression profiles of T cells family. Wilcox. test was used for differential estimation on immune infiltration. The P value cutoff was 0.05.

2.8. Tumor immune dysfunction and rejection (TIDE) algorithm

We adopted the TIDE algorithm (http://tide.dfci.harvard.edu/) to predict the immunotherapy efficiency to checkpoint blockade between clusters [27]. Cells limiting T cell infiltration in tumors, such as tumor associated macrophages (TAM), myeloid derived suppressor cells (MDSCs) and tumor associated fibroblasts (CAF) were evaluated. Tumor infiltration cytotoxic T lymphocyte (CTL) dysfunction, indicating tumor immune escape indicator were also calculated. Wilcox. test was used to produce the *P* value between clusters for differential estimation on immune infiltration. The *P* value cutoff was 0.05.

2.9. Cell culture

Human gastric mucosal epithelial cells (GES-1) as well as human GC cells (SNU484 and Hs746t) (American Type Culture Collection (ATCC)) were cultivated in RPMI-1640 (Gibco) plus 10 % fetal bovine serum (FBS; Gibco) with 1 % penicillin-streptomycin solution (Yeasen). All cells were grown in an atmosphere with 5 % CO_2 at 37 °C.

2.10. Quantitative real-time PCR (qPCR)

The isolation of total RNA was carried out using TRIzol solution (Sigma-Aldrich), followed by antisense transcription into complementary DNA using PrimeScript RT Master Mix (Takara) and 7500 Real-Time PCR System (Applied Biosystems). Subsequently, qPCR was conducted with SYBR qPCR Master Mix (Takara), and the following primers were utilized: MUC2 (5′-GAGGGCA-GAACCCGAAACC-3' (sense), 5′-GGCGAAGTTGTAGTCGCAGAG-3' (antisense)), MUC15 (5′-TATTCACTTCTATCGGGGAGCC-3' (sense), 5′-GGGAATGACTCGCCTTGAGAT-3' (antisense)), MUC19 (5′-TTACCACTGGGATAACTACTGGC-3' (sense), 5′-GCCTCTGTAAGAGCAAATCAAGA-3' (antisense)), MUC20 (5′-ATGACAACGGACGACACAGAA-3' (sense), 5′-TCAGCGTTTGAGTTTC-CAGAG-3' (antisense)), and GAPDH (5′-CTGGGCTACACTGAGCACC-3' (sense), 5′-AAGTGGTCGTTGAGGGCAATG-3' (antisense)). The quantification of relative expression values was performed using 2-ΔΔCt, where GAPDH served as an endogenous reference.

2.11. Western blotting

The protein extraction process began with the use of RIPA reagent (Thermo Fisher) and protease/phosphatase inhibitors (Thermo Fisher) on ice for 30 min. Subsequently, the protein concentration was determined using the BCA Protein Assay Kit (Pierce). Following this, 20 μg of the proteins were loaded onto SDS-PAGE gels and transferred to PVDF membranes (Millipore). The membranes were then incubated in 5 % BSA for 1 h, after which they were exposed to primary antibodies against MUC15 (abs101729; Absin; 1:1000), MUC19 (ab123813; Abcam; 1:2000), MUC20 (ab231659; Abcam; 1:2000) or GAPDH (ab181602; Abcam; 1:15,000) at 4 °C overnight, and subsequently with HRP-conjugated secondary antibody (ab288151; Abcam; 1:2000) for 2 h at room temperature. Finally, the protein blots were exposed using enhanced chemiluminescence reagent (Millipore), and the grey values were quantified using ImageJ software.

2.12. Transfection

When the cellular density reached 60–70 %, gene knockdown was performed by transfecting specific small interfering RNAs (siRNAs) targeting MUC15 (si-MUC15) or MUC20 (si-MUC20) (GenePharma) into cells using Lipofectamine 3000 (Invitrogen) according to the manufacturer's instructions.

2.13. Immunofluorescent staining

The experiment began with the cultivation of cells on glass cover slips in 24-well plates. The following day, the cell medium was removed, and the cells were fixed with 4 % paraformaldehyde (Thermo Fisher) and then permeabilized with 0.01 % Triton X-100 (Beyotime) for 15 min. The slides were then sealed with 1 % BSA/PBS before being exposed to primary antibodies against MUC15 (abs101729; Absin; 1:200), MUC20 (ab231659; Abcam; 1:100), E-cadherin (ab40772; Abcam; 1:100), or N-cadherin (ab18203;

Abcam; 1:100) overnight at 37 °C away from light. Following this, the slides underwent incubation with Alexa Fluor® 488 (ab150077; Abcam; 1:200) or Alexa Fluor® 647 (ab150079; Abcam; 1:250) secondary antibody. Subsequently, cell counterstaining with DAPI was performed for 30 min. Finally, the fluorescence distribution and intensity were examined under an immunofluorescence microscope (Olympus).

2.14. Cell counting kit 8 (CCK-8) assay

Cell viability was tested via CCK-8 kit (Yeasen) based upon the manufacturer's procedures. Cells were cultivated in 96-well plates (1*104 cells/well). After 2 days, they were administrated with 10 μL CCK-8 reagent lasting 2 h at 37 °C. Utilizing a microplate reader (BioTek), the absorbance values were detected at 450 nm.

2.15. Wound healing assay

Cells were cultivated on 6-well plates (5*104 cells per well). When the cellular confluence was ~90 %, scratches were made via a pipettor tip and the detached cells were rinsed by PBS. Subsequently, cells were cultivated in media without FBS lasting 24 h. The scratches were separately captured at 0 h and 24 h with an inverted microscope (Olympus).

2.16. Statistical analysis

Spearman correlation was applied to calculate the correlation coefficients between the hub genes. Wilcoxon test and Kruskal–Wallis test were applied to separately conduct the group comparisons of 2 groups and more than 2 groups. Overall survival curves were generated using the Kaplan–Meier method, and the group comparisons were performed with the log-rank test. All experimental data were displayed as the mean ± standard deviation, and analyzed via GraphPad Prism (v 9.0.1). Statistical analysis of two groups was evaluated via Student's t-test. One-way ANOVA was adopted to compare three groups. $P < 0.05$ was statistically significant.

3. Results

3.1. Map of differentially expressed genes and genetic alteration in MUCIN, CLDN and ZNF family

In the STAD cohort, 375 samples were analyzed, with 63 diagnosed with diffuse-type gastric cancer and 5 normal tissue samples serving as control. Utilizing the Limma package and counts data, a differential expression analysis was conducted, identifying a total of 17,687 differentially expressed genes, with 2822 upregulated and 2478 downregulated under the conditions of FC≥2 and $P < 0.05$ (Fig. 1A). Additionally, the heat-map depicted the top 20 most differentially expressed genes (Fig. 1B).
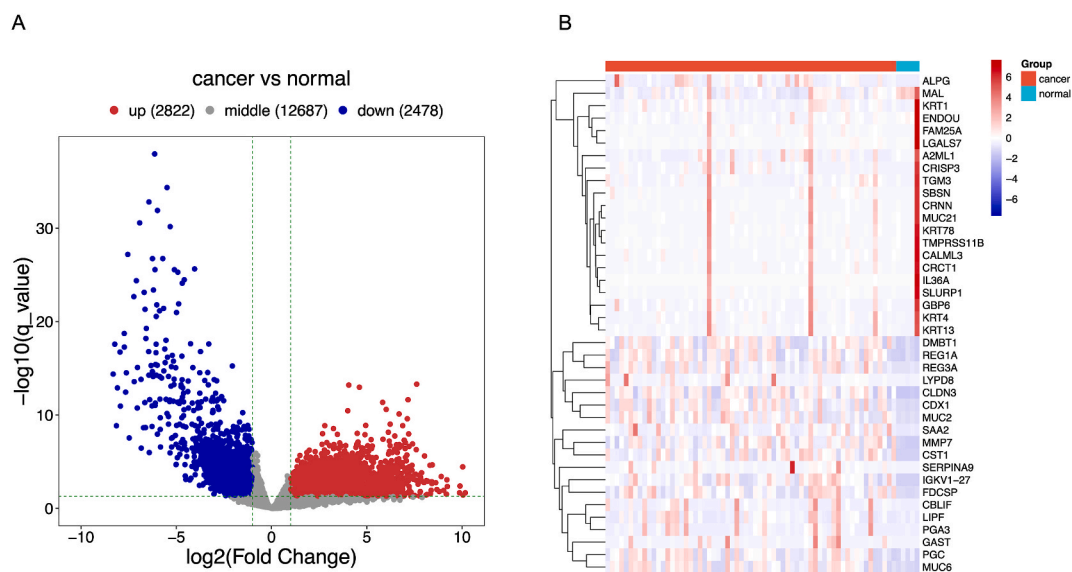

Fig. 1. The DEGs and their distributions between normal and tumor tissue. A. Volcano plot showed upregulated and down regulated genes between normal and tumor tissues. B. Heatmap showed top 20 genes upregulated and downregulated between normal and tumor tissues.

3.2. The relationship between MUCIN expression and its prognostic role in DGC

Our findings, illustrated in Fig. 2, S1, and S2, highlighted the MUC, ZNF, and CLDN families, respectively. Notably, the univariable Cox analysis revealed significant prognostic potential in genes of the MUC and CLDN families, with specific genes such as CLDN11 (P = 0.03779, HR = 1.291), CLDN34 (P = 0.02257, HR = 1.466), CLDN9 (P = 0.00430, HR = 1.284), MUC15 (P = 0.008, HR = 1.226), MUC19 (P = 0.011, HR = 1.228), and MUC2 (P = 0.029, HR = 1.11) being notable (Fig. 3A). Notably, the MUCIN family emerged as significantly relevant, prompting us to select MUCIN genes with positive univariable Cox results for further multivariable analysis. Subsequently, our multivariable Cox analysis, depicted in Fig. 3B, revealed that MUC15 (P = 0.008, HR 1.23, 95%CI 1.05–1.43), MUC19 (P = 0.011, HR 1.23, 95%CI 1.05–1.44), MUC2 (P = 0.029, HR 1.11, 95%CI 1.01–1.21), and MUC20 (P = 0.032, HR 1.25, 95% CI 1.02–1.54) exert a negative influence on overall survival.
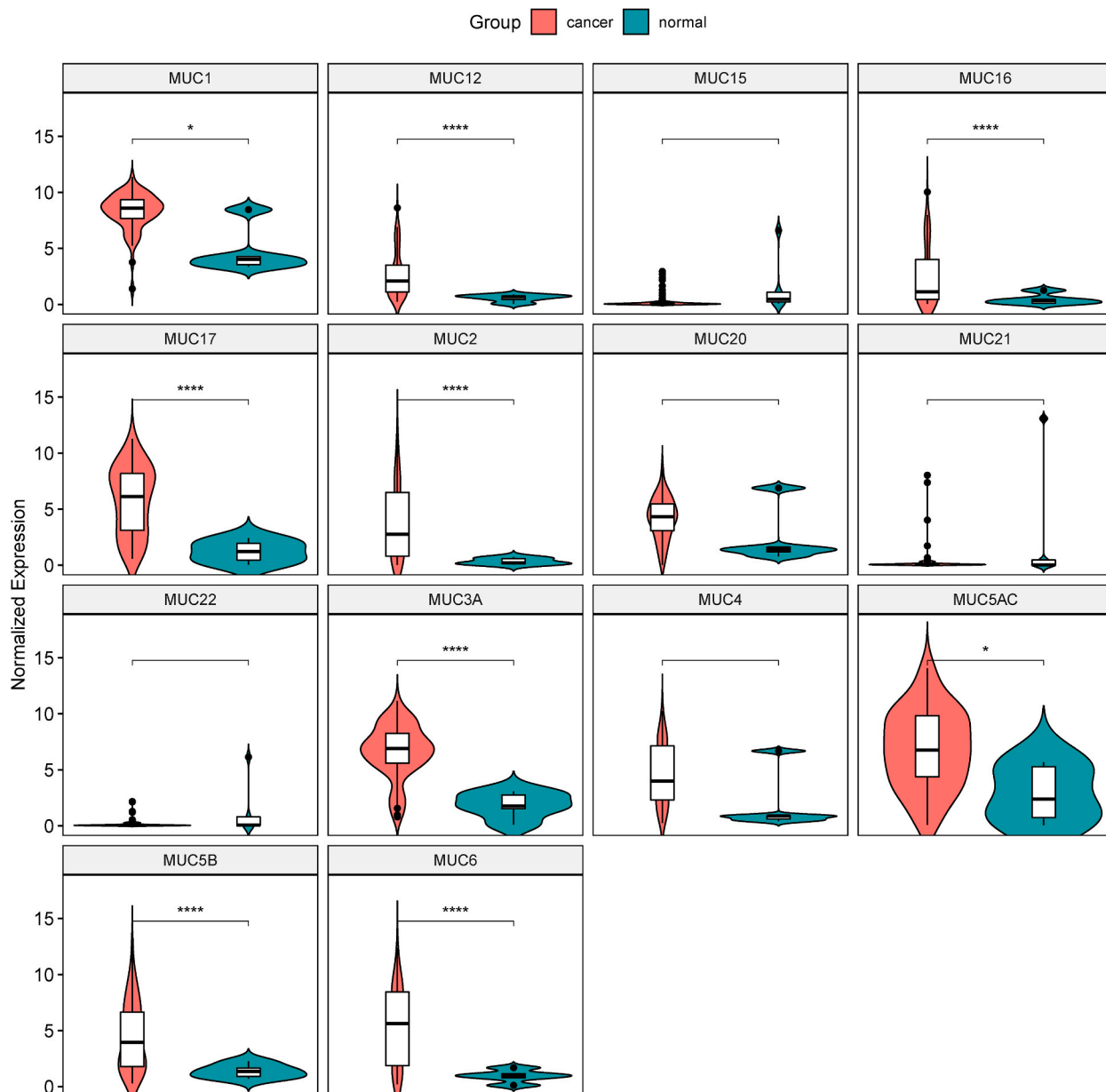

Fig. 2. Relative mRNA expression levels in DGC and normal tissues. A. Membrane-bound MUCINs (MUC1, MUC3A, MUC4, MUC12, MUC15, MUC16, MUC17, MUC20, MUC21, and MUC22) and secreted MUCINs (MUC2, MUC5AC, MUC5B, MUC6) were labeled with red and blue titles, respectively. Statistical analyses were performed using unpaired *t*-test. *P ≤ 0.05, **P ≤ 0.01, ***P ≤ 0.001.
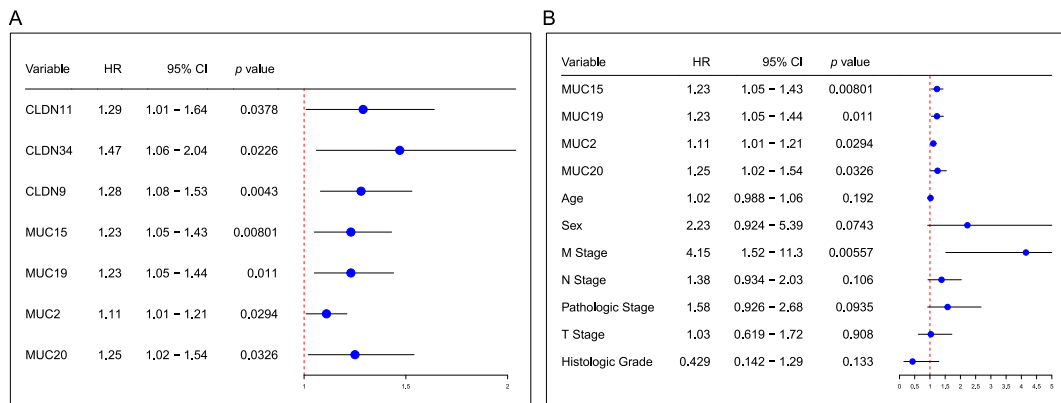
Fig. 3. Identification of prognostic-related genes. A. Univariate Cox analyses showed the hazard ratios (HRs) of selected CLDN and MUNCIN genes with forest plot. B. Multivariate Cox regression analyses showed four selected MUCIN genes and clinicopathological features in DGC patients.

3.3. The result of clustering analysis and nomogram analysis

After consensus clustering of the subtypes in this cohort, we identified 2 clusters based on the expression levels of MUC15, MUC19, MUC2, and MUC20 (Fig. 4A–C). Subsequently, Kaplan-Meier analysis revealed that cluster 2 exhibited a significantly better disease-free-survival (P = 0.021) and overall-survival (P = 0.011) compared to cluster 1, suggesting distinct prognostic implications for the clusters (Fig. 4E). Following this, ROC curve analysis was performed to estimate the prediction probability for each candidate gene (Fig. 5A–D). The AUC values for MUC2 and MUC20 were calculated and indicated that both had AUCs above 0.7 for 1-year survival prediction, demonstrating their high predictive value for prognosis. Moreover, the analysis of clinical characteristics between clusters, presented in Fig. S3, yielded statistically insignificant results. Subsequent to the multivariable analysis, the expression of MUC2, MUC15, MUC19, MUC20, and M stage were used to construct a nomogram for survival prediction (Fig. 5E). In the nomogram model, the total score was derived from the summation of individual scores for each variable, enabling the prediction of probable survival rate based on the total points. Furthermore, ROC curve analysis indicated that the nomogram model exhibited satisfactory predictive ability for 1-year survival (Fig. 5G). The total score was further stratified into low-risk and high-risk groups, with patients below the median risk score considered as the low-risk group, and the opposite as the high-risk group. Subsequently, Kaplan-Meier analysis
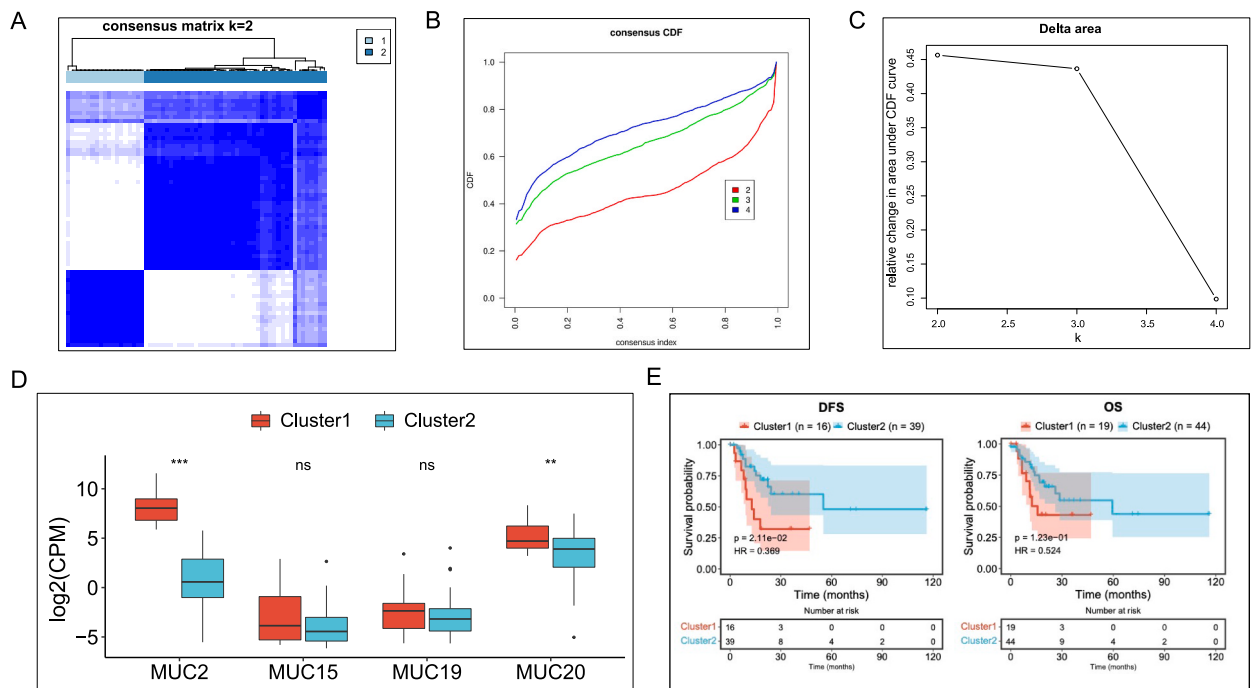

Fig. 4. Identification of clusters. A. Heat map of sample clustering. B. Cumulative distribution function curve. C. Delta area of related genes. D. Expression of targeted MUNCINs between clusters E. Survival curves of cluster1 and cluster2 in test cohort.
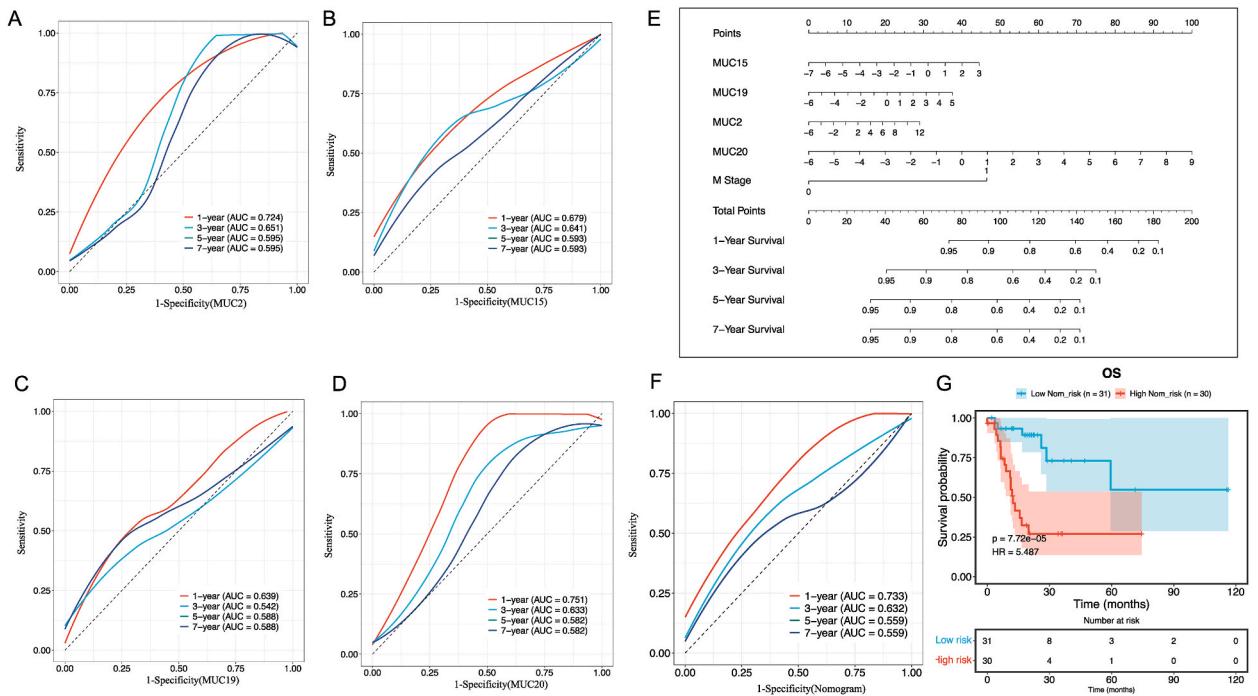
Fig. 5. Construction and validation of predicting model for overall survival. A.-D. Receiver operating characteristic (ROC) curve of 1,3,5 and 7 years of selected MUCINs. E. Nomogram showed the potential prognostic role for four selected MUCINs. F. Receiver operating characteristic (ROC) curve of 1,3,5 and 7 years of nomogram model. G. Kaplan–Meier survival curve showed the overall survival in two clusters.

revealed that the low-risk group had significantly better overall-survival than the high-risk group, validating the performance of the nomogram model (Fig. 5F).

3.4. MUCIN signature and different characteristics between clusters in immune activity

Upon conducting GSEA analysis to compare the biological behaviors of two clusters, we identified the mechanism responsible for the poor prognosis in cluster 1. Subsequently, KEGG pathway analysis revealed that cluster 1 was markedly enriched in
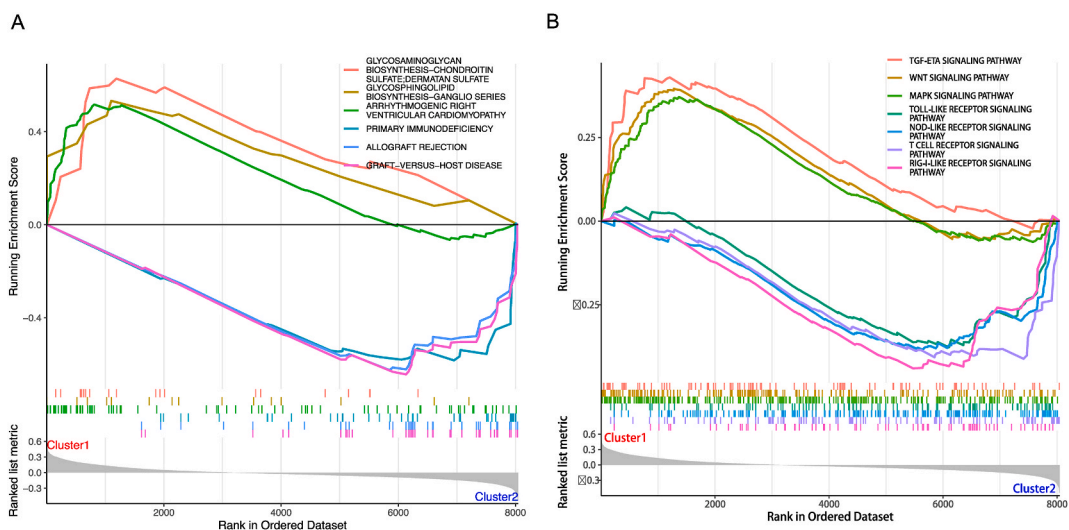

Fig. 6. Comparison of various metabolic patterns of DGC. A. GSEA analysis of top 6 metabolic patterns between clusters. B. GSEA analysis of top 6 most immune-related biological pathways between clusters. The TGF-beta, WNT, and MAPK signaling pathways were up-regulated in high-MUC20-expression cluster.

glycosaminoglycan biosynthesis and glycosphingolipid, while cluster 2 exhibited enrichment in primary immunodeficiency, allograft rejection, and graft-versus-host disease (Fig. 6A and B). Further, MF analysis demonstrated that cluster 1 was markedly enriched in transforming-growth factor beta binding and muscle alpha-actinin binding, while cluster 2 was enriched in single-stranded DNA helicase activity and MHC protein binding (Fig. S4A). Additionally, BPs showed that cluster 1 was markedly enriched in regulation of WNT signaling pathway and membrane repolarization, while cluster 2 was enriched in regulation of natural killer cell-mediated immunity and positive regulation of natural killer cell-mediated immunity (Fig. S4B). Moreover, CCs indicated that cluster 1 was markedly enriched in presynaptic active zone membrane, whereas cluster 2 was enriched in T cell receptor complex and nucleosome (Fig. S4C). These findings collectively denote a discernible difference in immunity between clusters. Our immune-related KEGG analysis further revealed that cluster 1 was markedly enriched in TGF-beta signaling pathway, WNT signaling pathway, and MAPK signaling pathway, while cluster 2 was enriched in T cell receptor signaling and RIG-I-LIKE receptor signaling pathway, suggesting varying immune activity between the clusters.

Upon further analysis of immune-related signatures in the two clusters, our results demonstrated that cluster 1, with higher expression of MUC20, exhibited a lower TMB than that of cluster 2, indicating limited benefits of immunotherapy (Fig. 7A and B). Additionally, the frequency of mutated genes in the clusters was reflected in Fig. 7C and D, revealing that TGFBR1, MAP2k, FGF9, JAKMIP1, KPNB1, PCDHGA12, PTCHD3, SLC12A5, TNRC6A were highly mutated genes in cluster 1 compared to cluster 2. Subsequently, we delved into the characteristics of immune activity and the proportion of immune cells in each cluster. The heatmap visualization showcased evident differences in the infiltration of immune cells, with the score of M0 macrophages of innate immune being higher in cluster 1 compared to cluster 2, and the abundance of $CD8^+$ T cells and activated $CD4^+$ memory T cell being increased in cluster 2, signifying a synergistic relationship between them (Fig. 8A, B, and 8C). Considering the pivotal role of immune checkpoints (ICPs) in anti-tumor immunity and their influence on the efficacy of immunotherapy, we assessed the expression of 20 ICPs in the two clusters, revealing higher expression of LGALS3 and CEACAM1 in cluster 1, and higher expression of PDCD1 (PD-1), KIR3DL1, LAG3, and TIGIT in cluster 2 (Fig. 9A). Furthermore, the result of T cell-inflamed score, which defines preexisting cancer immunity and predicts the clinical response of immune checkpoint blockade (ICB), indicated higher scores in cluster 2 (Fig. 9C), while TIDE score estimation revealed a lower score in cluster 1, implying a higher tumor immune escape probability, limited benefits of immune therapies, and poor prognosis, consistent with the TMB results (Fig. 9D and E). Moreover, further analysis of immune correlation with targeted MUCIN family in DGC found a positive correlation between MUC 20 and the infiltration of various immune cells, including M2 macrophages and regulatory T cells, and a negative correlation with M1 macrophages, activated memory $CD4^+$ T cell, follicular helper T cell, and resting NK cells. Additionally, MUC20 was positively associated with immune checkpoints, such as VTCN1, CEACAM1, and CD276, and negatively associated with TIGIT, PDCD1, LAG3, IDO1, CTLA4, CD80, CD274, and ADORA2A, suggesting that MUC20 may hold crucial prognostic value and offer insights into immunotherapy for DGC.
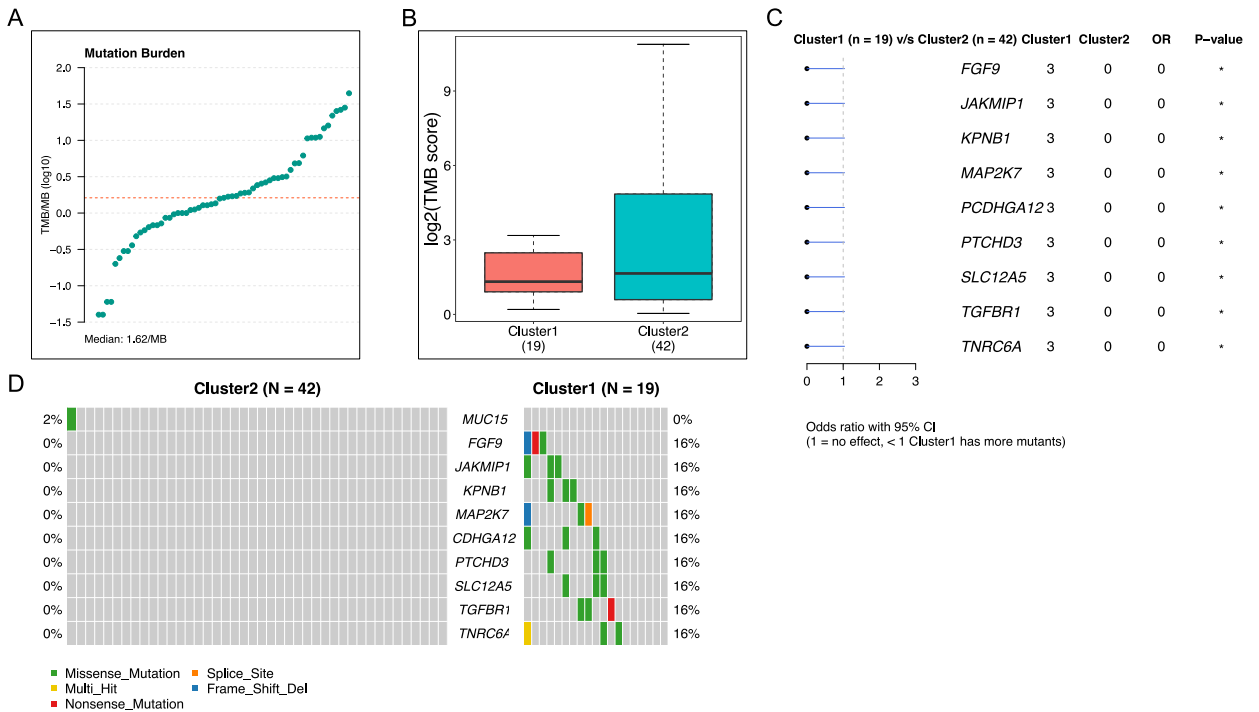

Fig. 7. Mutation burden and CNV analysis. A.-B. Barplot showed tumor mutation burden between clusters. C.-D. Numbers of mutation genes and CNV analysis between clusters.
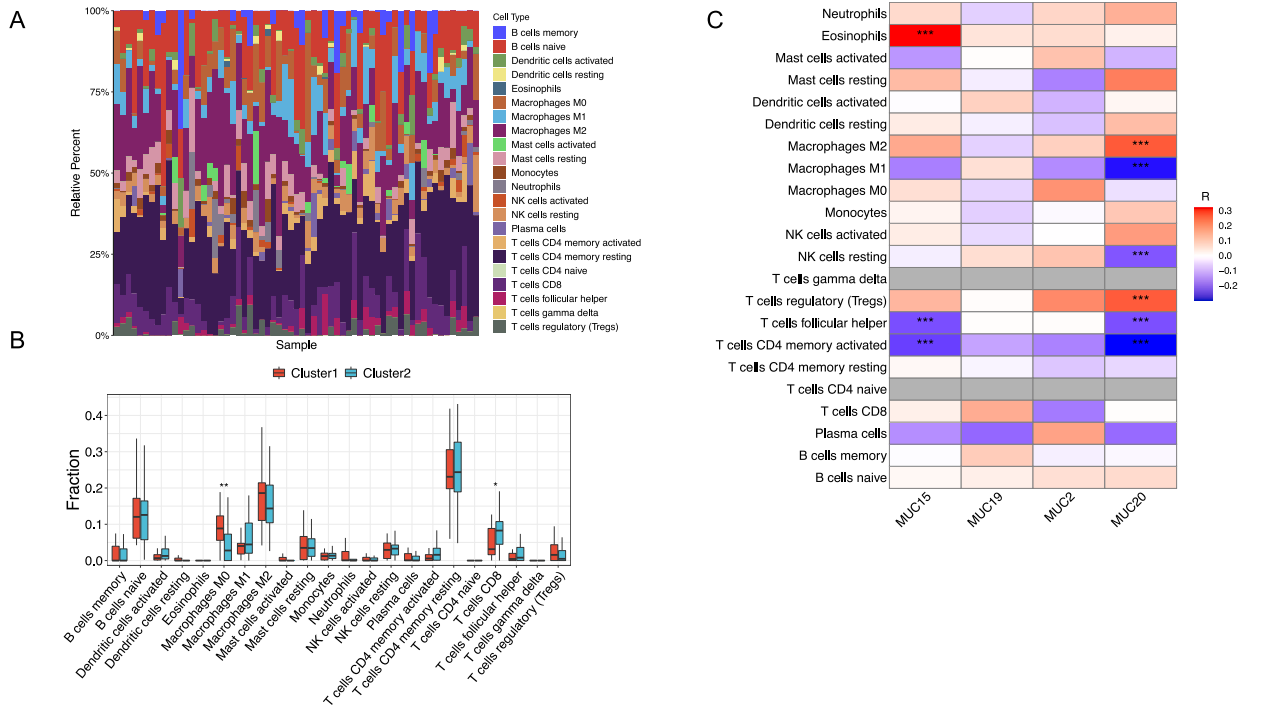
Fig. 8. Immune cell infiltration pattern in tumor and normal tissue. A. Barplot showed the distribution of 22 immune cells in tumor samples. B. Boxplot showed the distribution of 22 immune cells in tumor tissue between clusters. C. Heatmap showed correlation between four targeted MUNICNs and the 22 immune cells infiltration in tumor tissue. ***p < 0.001, **p < 0.01, *p < 0.05, ns p > 0.05.
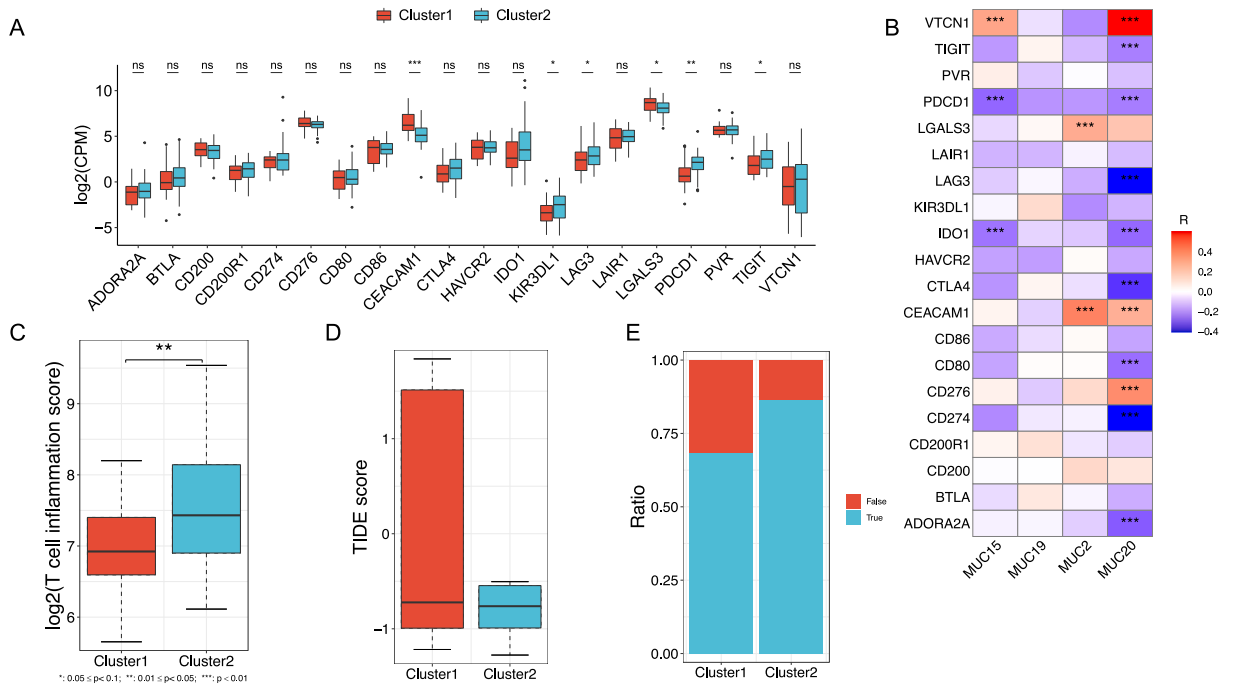

Fig. 9. Distributions of ICBs between clusters. A. Boxplot showed expression of ICBs between clusters. B. Heatmap showed correlation between four targeted MUNICNs and ICBs in tumor tissue. C. Boxplot showed T-cell inflammation score between clusters. D-E. Boxplot showed wilcox. test and chisq. test of TIDE score between clusters. ***p < 0.001, **p < 0.01, *p < 0.05, ns p > 0.05.

3.5. Experimental validation of aberrantly expressed MUCIN family members in GC cells

The expressed levels of MUCIN family members: MUC2, MUC15, MUC19, and MUC20 in gastric mucosal epithelial cells (GES-1) as well as GC cells (SNU484 and Hs746t) were experimentally verified in this study. Our qPCR results revealed that MUC2 expression did not show a statistically significant difference in SNU484 and Hs746t cells compared to GES-1 cells (Fig. 10A). Conversely, MUC15, MUC19, and MUC20 exhibited significant up-regulation in the two GC cell lines compared to GES-1 cells (Fig. 10B–D). Subsequently, we conducted a Western blot analysis to measure the expression of MUC15, MUC19, and MUC20. The results indicated notable overexpression of MUC15 and MUC20 in the GC cells as compared to GES-1 cells, while no differential difference in MUC19 expression was observed (Fig. 10E–H). Consistent with previous studies [28], our findings confirm the overexpression of MUC15 and MUC20 in GC cells.

3.6. Both knockdown of MUC15 and MUC20 restrained cell viability and migration of GC cells

The study aimed to validate the precise roles of MUC15 and MUC20 in the biology of gastric cancer (GC) cells. To achieve this, specific siRNAs targeting MUC15 or MUC20 were transfected into SNU484 and Hs746t cells. Immunofluorescence analysis confirmed a remarkable suppression of MUC15 and MUC20 in the GC cells compared to the control group (Fig. 11A–D). Following this, cell viability was assessed using the CCK-8 assay, which revealed significantly reduced viability in MUC15- or MUC20-silenced SNU484 and Hs746t cells (Fig. 11E and F). Moreover, the data from the wound healing assay demonstrated a notable hindrance in the migration of SNU484 and Hs746t cells upon MUC15 or MUC20 knockdown (Fig. 11G–J). Combined, these results indicate that therapeutic targeting of MUC15 or MUC20 has the potential to restrain the growth and migration of GC cells.
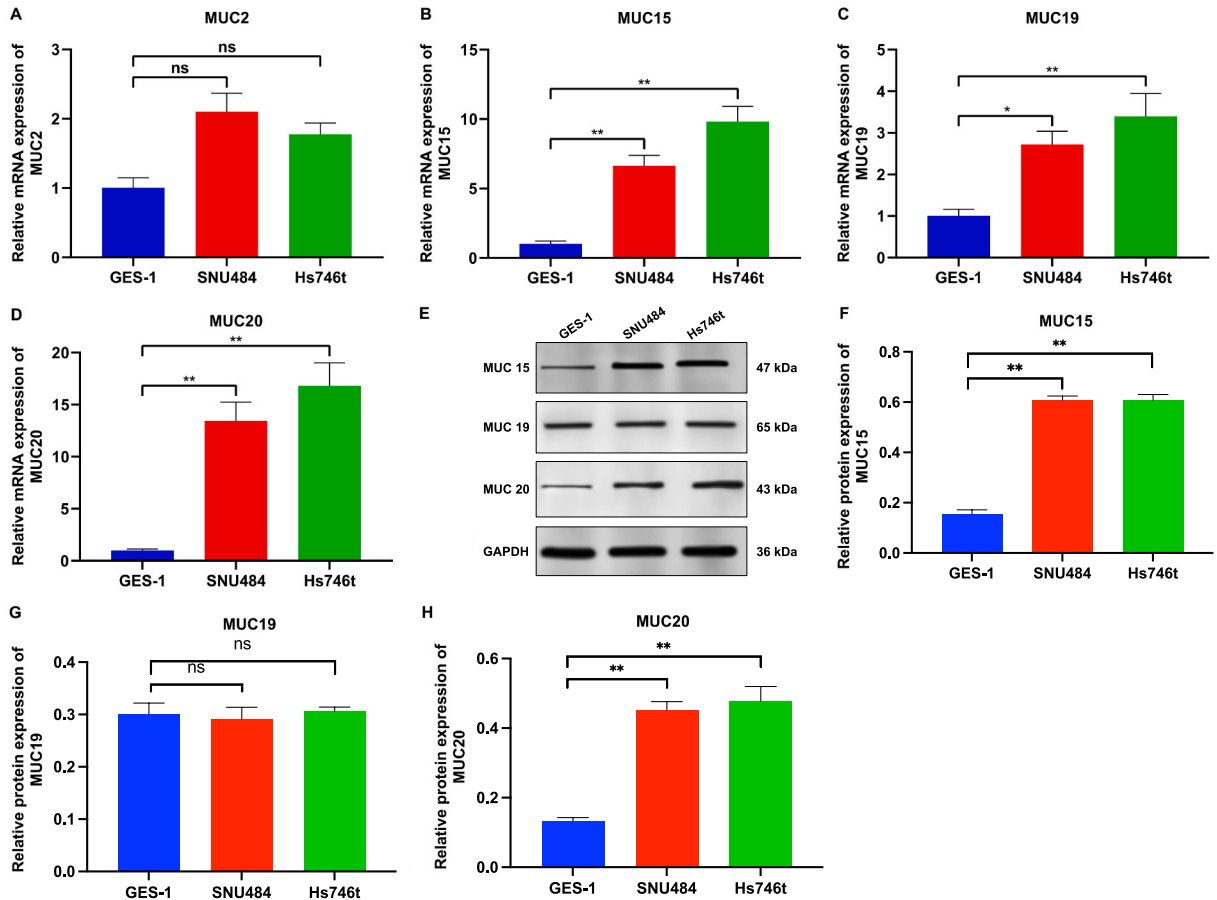

Fig. 10. Experimental verification of dysregulated expression of MUCIN family members in GC cells. (A–D) Detection of mRNA levels of (A) MUC2, (B) MUC15, (C) MUC19 and (D) MUC20 in GES-1, SNU484 and Hs746t cells through qPCR. (E) Representative Western blot images of MUC15, MUC19 and MUC20 in GES-1, SNU484 and Hs746t cells, raw data in supplementary materials FigureS 5 A-D. GAPDH was served as an internal reference. (F–H) Quantification of protein levels of (F) MUC15, (G) MUC19 and (H) MUC20 in GES-1, SNU484 and Hs746t cells based upon protein bands. *P < 0.05; **P < 0.01; ns: no statistical significance.
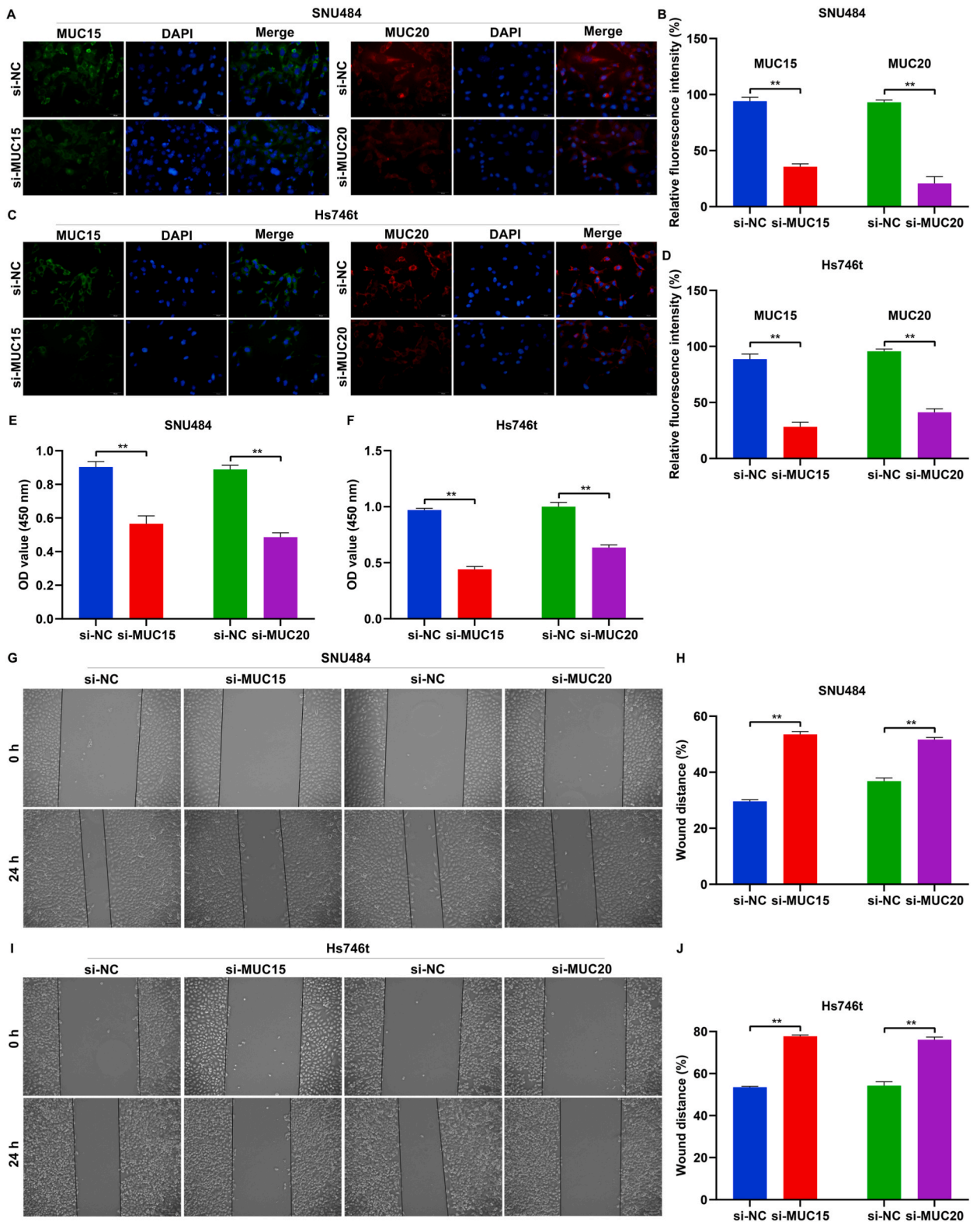
(caption on next page)

Fig. 11. Effects of MUC15 and MUC20 knockdown on cell viability and migratory abilities of GC cells. (A) Representative immunofluorescence photographs of MUC15 and MUC20 in SNU484 cells in the context of transfection of si-MUC15, si-MUC20 or controls. Scale bar, 20 μm. (B) Quantification of fluorescence intensity of MUC15 and MUC20 in the figure above. (C, D) Representative immunofluorescence photographs of MUC15 and MUC20 and quantification results in Hs746t cells transfected with si-MUC15, si-MUC20 or controls. (E, F) Detection of OD values at 450 nm in SNU484 and Hs746t cells in the context of si-MUC15, si-MUC20 or control transfection by CCK-8 assay. (G) Representative wound healing photographs of SNU484 cells under transfection of si-MUC15, si-MUC20 or controls at 0 h and 24 h. Scale bar, 50 μm. (H) Calculation of wound distance (%) in the figure above. (I, J) Representative 0- and 24-h wound healing images in Hs746t cells transfected with si-MUC15, si-MUC20 or controls as well as quantification of wound distance (%). **P < 0.01.

3.7. *Both knockdown of MUC15 and MUC20 suppressed epithelial-to-mesenchymal transition (EMT) process in GC cells*

EMT is essential for invasive and metastatic cancer cell spreading [21]. Thus, we focused on the influence of MUC15 and MUC20 on EMT process. The immunofluorescence results demonstrated that E-cadherin expression was remarkably up-regulated by MUC15 or MUC20 knockdown both in SNU484 and Hs746t cells (Fig. 12A–D). It was also found the reduced expression of N-cadherin in MUC15- or MUC20-silenced SNU484 and Hs746t cells (Fig. 12E–H). Combining with prior studies [29–31], our findings unveil that MUC15 and MUC20 participate in mediating EMT process of GC cells.

4. Discussion

In this study, we focused on the analysis of MUCINs, which are O-glycoproteins primarily expressed by epithelial cells and are
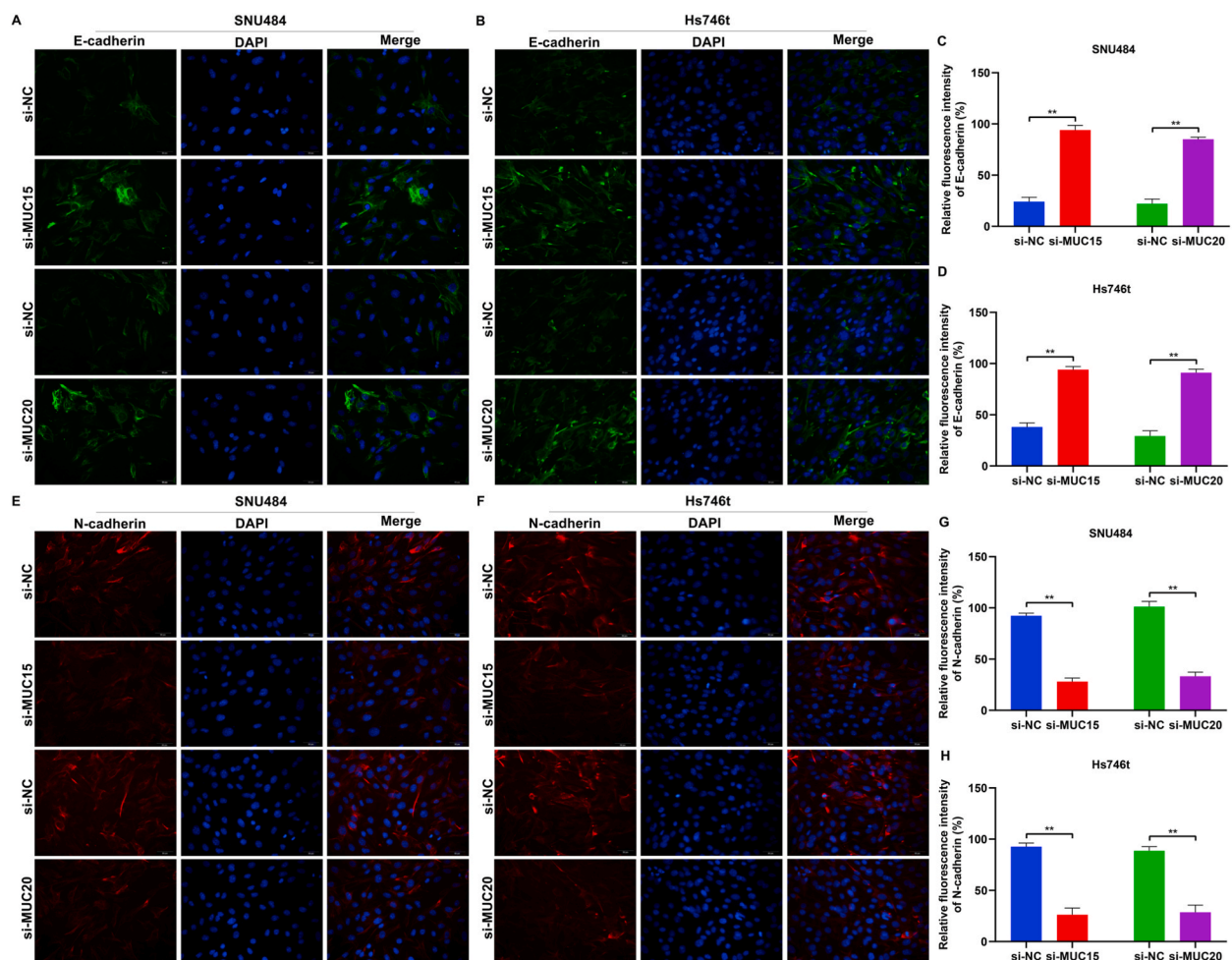
Fig. 12. Effects of MUC15 and MUC20 knockdown on EMT process in GC cells. (A, B) Representative immunofluorescence photographs of E-cadherin in SNU484 and Hs746t cells in the context of si-MUC15, si-MUC20 or control transfection. Scale bar, 20 μm. (C, D) Calculation of fluorescence intensity of E-cadherin in the figures above. (E–H) Representative immunofluorescence photographs and fluorescence intensity of N-cadherin in SNU484 and Hs746t cells with si-MUC15, si-MUC20 or control transfection. **P < 0.01.

categorized into secreted, membrane-bounded, and atypical types [32].Although the secreted and membrane-bounded types of MUCINs have been implicated in facilitating oncogenic processes in various malignancies, the relationship between the expression levels of MUCINs and the prognosis of patients with diffuse gastric cancer (DGC) remains ambiguous [32–34]. To address this gap, we gathered DGC data from the TCGA database and conducted an analysis of MUCINs' correlation with clinical outcomes. Notably, our analysis revealed the existence of two distinct clusters based on the expression levels of MUCIN2, MUCIN15, MUCIN19, and MUCIN20, and their association with clinical outcomes. Notably, cluster 2, characterized by lower expression of MUCIN2 and MUCIN20, was found to be associated with a more favorable survival outcome.

MUCIN2 is one of the secreted MUCINs, and it is commonly overexpressed in mucinous adenocarcinomas, particularly in CRCs. These tumors are associated with mutation of KRAS and BRAF [35], and displaying microsatellite instability [36], leading to a greater tendency of recurrence and metastasis [37]. The clinical significance of MUC2 as a diagnostic marker and prognostic factor in CRC is supported by several lines of evidence. A systemic meta-analysis involving 6032 CRC patients revealed a link between increased MUC2 expression and prolonged overall survival [38]. There is a lack of research focusing on MUC19, another secreted mucin, except for an interesting finding that long non-coding RNA A2M-AS1 promotes breast cancer through the upregulation of MUC19 [39]. Although MUCIN15, a highly glycosylated protein found in the small intestine, colon, and liver [40], has not been reported in GC, further investigation regarding its specific role is necessary.

MUCIN20, a membrane-bound mucin, has been correlated with enriched immune-related activities in ccRCC, indicating its role in tumor microenvironment modulation [41]. Moreover, MUC20-overexpressing GC cells have been found to exhibit chemoresistance to cisplatin and paclitaxel, suggesting a potential role as a target for reversing drug resistance [28]. Our experiments in vitro have demonstrated overexpression of MUC20 on GC cells and its positive relationship with EMT viability, suggesting its involvement in tumor metastasis and a potential therapeutic target.

The results of GSEA analysis revealed differences in immune activity between clusters. Cluster 1 was notably enriched in transforming-growth factor beta (TGF-β) and WNT signaling, associated with poor prognosis. It is reported that c-Jun/TGF-β signaling contributes to the progression of RCC by increasing RCC cell growth and cell invasion [42,43]. Additionally, WNT and TGF-β signaling have been found to cooperate in inducing tumorigenesis in gastric cancer, suggesting the potential value of targeting this crosstalk for therapeutic intervention in DGC [44].

With the advancements in genome technologies and targeted therapies, three approved strategies are recommended by guidelines for cancer treatment: trastuzumab targeted at HER2 [7,45,46], ramucirumab targeted at VEGF2 [47], and nivolumab and pembrolizumab, ICIs targeted at PD-1 [48].In the last decade, cancer immunotherapy has emerged as a milestone in cancer treatment, including checkpoint inhibitors, adoptive immune cell therapy, and cancer vaccines. GC of EBV + or MSI subtype with high expression of immune checkpoints are promising candidates for cancer immunotherapy according to TCGA classification.

In our study, we observed that cluster 2, with lower expression of MUC2 and MUC20, has a higher tumor mutation burden (TMB) and higher TIDE score than cluster 1, indicating its potential benefit from immunotherapy. Additionally, we found that cluster 2 had better prognosis with less M0 macrophages and more CD8$^+$ T-cell infiltrate. Similarly, longer survival is associated with greater CD8$^+$ T-cell infiltrate and the presence of M1 macrophages in tumors. Furthermore, higher baseline CD8$^+$ T-cell infiltrate indicates a stronger response to *anti*-PD1 treatment [49–52]. Moreover, the expression of MUC20 in cluster 2 is positively related to M2 macrophage and regulatory T cell infiltration, along with lower levels of surface molecules associated with T cell activation, such as LAG-3 and TIGHT. Targeting surface molecules on Tregs, such as CTLA-4, CD25, OX-40, LAG3, and TIGIT, may help control tumor burden [53,54]. Based on the expression of MUCINs, we identified two clusters with different clinical outcomes and distinct immune characteristics, and developed a nomogram model for prediction in this study. Notably, MUC20 was found to be an independent prognostic factor and correlated with the levels of ICBs and immune cell infiltration in the tumor, indicating its potential role as an immune therapy indicator. However, our study has certain limitations. Firstly, it is a small retrospective study based on public data with some clinical details missing, such as adjuvant therapies and recurrence patterns. Secondly, a validation set of DGC is needed to confirm our nomogram model, which should be further validated by prospective studies in the future.

In conclusion, we have successfully identified 2 clusters in DGC with distinct clinical and immune characteristics and constructed a nomogram model based on the expression of MUCINs. Furthermore, MUC20, which is correlated with EMT viability, clinical outcomes, and immune activity, has the potential to serve as a valuable prognostic factor for DGC. This suggests that it may provide a better therapy choice for DGC patients and could be considered as a potential clinical target.

Data availability statement

All data materials are published in the manuscript and supplementary materials are available on the journal website.

Role of funding source

CRediT authorship contribution statement

Xiao-Xiao Luo: Writing – original draft, Methodology. **Shi-Zhen Li:** Software, Investigation, Formal analysis. **Lu Wang:** Visualization, Validation, Project administration. **Ai-Lin Luo:** Writing – review & editing, Validation, Resources. **Hong Qiu:** Methodology, Conceptualization. **Xiang-Lin Yuan:** Writing – review & editing, Supervision, Conceptualization.

Declaration of competing interest

The authors declare the following financial interests/personal relationships which may be considered as potential competing interests:Xiao-Xiao Luo reports financial support was provided by Hubei Provincial Natural Science Foundation of China (grants 2023AFB208). If there are other authors, they declare that they have no known competing financial interests or personal relationships that could have appeared to influence the work reported in this paper.

Acknowledgments

The authors all thank TCGA for sharing the data.

Appendix A. Supplementary data

Supplementary data to this article can be found online at https://doi.org/10.1016/j.heliyon.2024.e31403.

References

[1] Y.C. Chen, W.L. Fang, R.F. Wang, et al., Clinicopathological variation of lauren classification in gastric cancer, Pathol. Oncol. Res. 22 (2016) 197–202.
[2] M. Cimerman, S. Repse, F. Jelenc, et al., Comparison of Lauren's, Ming's and WHO histological classifications of gastric cancer as a prognostic factor for operated patients, Int. Surg. 79 (1994) 27–32.
[3] Cancer Genome Atlas Research N, Comprehensive molecular characterization of gastric adenocarcinoma, Nature 513 (2014) 202–209.
[4] R. Cristescu, J. Lee, M. Nebozhyn, et al., Molecular analysis of gastric cancer identifies subtypes associated with distinct clinical outcomes, Nat. Med. 21 (2015) 449–456.
[5] Y. Chen, Y. Liang, Y. Chen, et al., Identification of prognostic metabolism-related genes in clear cell renal cell carcinoma, JAMA Oncol. (2021) 2042114, 2021.
[6] V. Thorsson, D.L. Gibbs, S.D. Brown, et al., The immune landscape of cancer, Immunity 48 (2018) 812–830 e14.
[7] A. Rizzo, V. Mollica, A.D. Ricci, et al., Third- and later-line treatment in advanced or metastatic gastric cancer: a systematic review and meta-analysis, Future Oncol. 16 (2020) 4409–4418.
[8] G. Pruneri, A. Vingiani, C. Denkert, Tumor infiltrating lymphocytes in early breast cancer, Breast 37 (2018) 207–214.
[9] H. West, M. McCleod, M. Hussein, et al., Atezolizumab in combination with carboplatin plus nab-paclitaxel chemotherapy compared with chemotherapy alone as first-line treatment for metastatic non-squamous non-small-cell lung cancer (IMpower130): a multicentre, randomised, open-label, phase 3 trial, Lancet Oncol. 20 (2019) 924–937.
[10] A.J. Muller, M.G. Manfredi, Y. Zakharia, et al., Inhibiting Ido pathways to treat cancer: lessons from the ECHO-301 trial and beyond, Semin. Immunopathol. 41 (2019) 41–48.
[11] A. Haslam, V. Prasad, Estimation of the percentage of US patients with cancer who are eligible for and respond to checkpoint inhibitor immunotherapy drugs, JAMA Netw. Open 2 (2019) e192535.
[12] F.S. Hodi, S.J. O'Day, D.F. McDermott, et al., Improved survival with ipilimumab in patients with metastatic melanoma, N. Engl. J. Med. 363 (2010) 711–723.
[13] J.D. Twomey, B. Zhang, Cancer immunotherapy update: FDA-approved checkpoint inhibitors and companion diagnostics, AAPS J. 23 (2021) 39.
[14] K. Rihawi, A.D. Ricci, A. Rizzo, et al., Tumor-associated macrophages and inflammatory microenvironment in gastric cancer: novel translational implications, Int. J. Mol. Sci. 22 (2021).
[15] Y. Liu, C. Li, Y. Lu, et al., Tumor microenvironment-mediated immune tolerance in development and treatment of gastric cancer, Front. Immunol. 13 (2022) 1016817.
[16] D.S. Vinay, E.P. Ryan, G. Pawelec, et al., Immune evasion in cancer: mechanistic basis and therapeutic strategies, Semin. Cancer Biol. 35 (Suppl) (2015) S185–S198.
[17] M.D. Robinson, D.J. McCarthy, G.K. Smyth, edgeR: a Bioconductor package for differential expression analysis of digital gene expression data, Bioinformatics 26 (2010) 139–140.
[18] A. Mayakonda, D.C. Lin, Y. Assenov, et al., Maftools: efficient and comprehensive analysis of somatic variants in cancer, Genome Res. 28 (2018) 1747–1756.
[19] J. Tu, M. Tang, G. Li, et al., Expression of mucin family proteins in non-small-cell lung cancer and its role in evaluation of prognosis, JAMA Oncol. (2022) 4181658, 2022.
[20] W.S. Kim, H. Kim, M.K. Joo, et al., High expression of claudin-4 is associated with synchronous tumors in patients with early gastric cancer, J. Clin. Med. 11 (2022).
[21] W. Wang, Z. Zhou, X. Dai, et al., LncRNA-ENST00000543604 exerts a tumor-promoting effect via miRNA 564/AEG-1 or ZNF326/EMT and predicts the prognosis of and chemotherapeutic effect in colorectal cancer, Front. Oncol. 12 (2022) 960481.
[22] M.D. Wilkerson, D.N. Hayes, ConsensusClusterPlus: a class discovery tool with confidence assessments and item tracking, Bioinformatics 26 (2010) 1572–1573.
[23] A.A. Rizvi, E. Karaesmen, M. Morgan, et al., gwasurvivr: an R package for genome-wide survival analysis, Bioinformatics 35 (2019) 1968–1970.
[24] M. Kanehisa, S. Goto, KEGG: kyoto encyclopedia of genes and genomes, Nucleic Acids Res. 28 (2000) 27–30.
[25] S. Hanzelmann, R. Castelo, J. Guinney, GSVA: gene set variation analysis for microarray and RNA-seq data, BMC Bioinf. 14 (2013) 7.
[26] B. Chen, M.S. Khodadoust, C.L. Liu, et al., Profiling tumor infiltrating immune cells with CIBERSORT, Methods Mol. Biol. 1711 (2018) 243–259.
[27] P. Jiang, S. Gu, D. Pan, et al., Signatures of T cell dysfunction and exclusion predict cancer immunotherapy response, Nat. Med. 24 (2018) 1550–1558.
[28] L. Fu, A. Yonemura, N. Yasuda-Yoshihara, et al., Intracellular MUC20 variant 2 maintains mitochondrial calcium homeostasis and enhances drug resistance in gastric cancer, Gastric Cancer 25 (2022) 542–557.
[29] X. Xiao, L. Wang, P. Wei, et al., Role of MUC20 overexpression as a predictor of recurrence and poor outcome in colorectal cancer, J. Transl. Med. 11 (2013) 151.
[30] T. Sasahira, M. Kurihara-Shimomura, H. Shimomura, et al., Identification of oral squamous cell carcinoma markers MUC2 and SPRR1B downstream of TANGO, J. Cancer Res. Clin. Oncol. 147 (2021) 1659–1672.
[31] S. Wu, Y. Yue, Y. Gu, et al., MUC15 loss facilitates epithelial-mesenchymal transition and cancer stemness for prostate cancer metastasis through GSK3beta/beta-catenin signaling, Cell. Signal. 84 (2021) 110015.
[32] R. Bhatia, S.K. Gautam, A. Cannon, et al., Cancer-associated mucins: role in immune modulation and metastasis, Cancer Metastasis Rev. 38 (2019) 223–236.
[33] B.I. Rini, B. Escudier, J.F. Martini, et al., Validation of the 16-gene recurrence score in patients with locoregional, high-risk renal cell carcinoma from a phase III trial of adjuvant sunitinib, Clin. Cancer Res. 24 (2018) 4407–4415.
[34] P. Kapur, S. Pena-Llopis, A. Christie, et al., Effects on survival of BAP1 and PBRM1 mutations in sporadic clear-cell renal-cell carcinoma: a retrospective analysis with independent validation, Lancet Oncol. 14 (2013) 159–167.

[35] L.J. Mekenkamp, K.J. Heesterbeek, M. Koopman, et al., Mucinous adenocarcinomas: poor prognosis in metastatic colorectal cancer, Eur. J. Cancer 48 (2012) 501–509.

[36] A.M. Wnorowski, C.O. Menias, P.J. Pickhardt, et al., Mucin-containing rectal carcinomas: overview of unique clinical and imaging features, AJR Am. J. Roentgenol. 213 (2019) 26–34.

[37] E.Y. Ko, H.K. Ha, A.Y. Kim, et al., CT differentiation of mucinous and nonmucinous colorectal carcinoma, AJR Am. J. Roentgenol. 188 (2007) 785–791.

[38] J. Betge, N.I. Schneider, L. Harbaum, et al., MUC1, MUC2, MUC5AC, and MUC6 in colorectal cancer: expression profiles and clinical significance, Virchows Arch. 469 (2016) 255–265.

[39] Y. Liu, Q. Zhang, J. Wu, et al., Long non-coding RNA a2m-AS1 promotes breast cancer progression by sponging microRNA-146b to upregulate MUC19, Int. J. Gen. Med. 13 (2020) 1305–1316.

[40] L.T. Pallesen, L. Berglund, L.K. Rasmussen, et al., Isolation and characterization of MUC15, a novel cell membrane-associated mucin, Eur. J. Biochem. 269 (2002) 2755–2763.

[41] B. Xue, W.M. Guo, J.D. Jia, et al., MUC20 as a novel prognostic biomarker in ccRCC correlating with tumor immune microenvironment modulation, Am. J. Cancer Res. 12 (2022) 695–712.

[42] S.L. Gao, R. Yin, L.F. Zhang, et al., The oncogenic role of MUC12 in RCC progression depends on c-Jun/TGF-beta signalling, J. Cell Mol. Med. 24 (2020) 8789–8802.

[43] Y. Sheng, C.P. Ng, R. Lourie, et al., MUC13 overexpression in renal cell carcinoma plays a central role in tumor progression and drug resistance, Int. J. Cancer 140 (2017) 2351–2363.

[44] S. Lei, A. Dubeykovskiy, A. Chakladar, et al., The murine gastrin promoter is synergistically activated by transforming growth factor-beta/Smad and Wnt signaling pathways, J. Biol. Chem. 279 (2004) 42492–42502.

[45] Y.J. Bang, E. Van Cutsem, A. Feyereislova, et al., Trastuzumab in combination with chemotherapy versus chemotherapy alone for treatment of HER2-positive advanced gastric or gastro-oesophageal junction cancer (ToGA): a phase 3, open-label, randomised controlled trial, Lancet 376 (2010) 687–697.

[46] A.D. Ricci, A. Rizzo, F.L. Rojas Llimpe, et al., Novel HER2-directed treatments in advanced gastric carcinoma: AnotHER paradigm shift? Cancers 13 (2021).

[47] C.S. Fuchs, J. Tomasek, C.J. Yong, et al., Ramucirumab monotherapy for previously treated advanced gastric or gastro-oesophageal junction adenocarcinoma (REGARD): an international, randomised, multicentre, placebo-controlled, phase 3 trial, Lancet 383 (2014) 31–39.

[48] A. Nakayama, H. Abe, A. Kunita, et al., Viral loads correlate with upregulation of PD-L1 and worse patient prognosis in Epstein-Barr Virus-associated gastric carcinoma, PLoS One 14 (2019) e0211358.

[49] C. Hu, B. Chen, Z. Huang, et al., Comprehensive profiling of immune-related genes in soft tissue sarcoma patients, J. Transl. Med. 18 (2020) 337.

[50] J. Deng, W. Zeng, W. Kong, et al., The study of sarcoma microenvironment heterogeneity associated with prognosis based on an immunogenomic landscape analysis, Front. Bioeng. Biotechnol. 8 (2020) 1003.

[51] H.Y. Gu, L.L. Lin, C. Zhang, et al., The potential of five immune-related prognostic genes to predict survival and response to immune checkpoint inhibitors for soft tissue sarcomas based on multi-omic study, Front. Oncol. 10 (2020) 1317.

[52] G. Viscardi, A.C. Tralongo, F. Massari, et al., Comparative assessment of early mortality risk upon immune checkpoint inhibitors alone or in combination with other agents across solid malignancies: a systematic review and meta-analysis, Eur. J. Cancer 177 (2022) 175–185.

[53] A. Tanaka, S. Sakaguchi, Targeting Treg cells in cancer immunotherapy, Eur. J. Immunol. 49 (2019) 1140–1146.

[54] Y. Bulliard, R. Jolicoeur, J. Zhang, et al., OX40 engagement depletes intratumoral Tregs via activating FcgammaRs, leading to antitumor efficacy, Immunol. Cell Biol. 92 (2014) 475–480.